Towards a minimal stochastic model for a large class of diffusion-reactions on biological membranes

Michael W. Chevalier and Hana El-Samad

Citation: The Journal of Chemical Physics **137**, 084103 (2012); doi: 10.1063/1.4746692
View online: http://dx.doi.org/10.1063/1.4746692
View Table of Contents: http://scitation.aip.org/content/aip/journal/jcp/137/8?ver=pdfcov
Published by the AIP Publishing

Towards a minimal stochastic model for a large class of diffusion-reactions on biological membranes

Michael W. Chevalier[a),c)] and Hana El-Samad[b),c)]
Department of Biochemistry and Biophysics, California Institute for Quantitative Biosciences, University of California San Francisco, 1700, 4th Street, San Francisco, California 94143-2542, USA

(Received 21 March 2012; accepted 2 August 2012; published online 23 August 2012)

Diffusion of biological molecules on 2D biological membranes can play an important role in the behavior of stochastic biochemical reaction systems. Yet, we still lack a fundamental understanding of circumstances where explicit accounting of the diffusion and spatial coordinates of molecules is necessary. In this work, we illustrate how time-dependent, non-exponential reaction probabilities naturally arise when explicitly accounting for the diffusion of molecules. We use the analytical expression of these probabilities to derive a novel algorithm which, while ignoring the exact position of the molecules, can still accurately capture diffusion effects. We investigate the regions of validity of the algorithm and show that for most parameter regimes, it constitutes an accurate framework for studying these systems. We also document scenarios where large spatial fluctuation effects mandate explicit consideration of all the molecules and their positions. Taken together, our results derive a fundamental understanding of the role of diffusion and spatial fluctuations in these systems. Simultaneously, they provide a general computational methodology for analyzing a broad class of biological networks whose behavior is influenced by diffusion on membranes. © *2012 American Institute of Physics*. [http://dx.doi.org/10.1063/1.4746692]

I. INTRODUCTION

Diffusion is a major transport mechanism for biological molecules. Most common is diffusion of proteins within the 3D medium of the cytosol or the 2D diffusive motion of membrane proteins on the surface of a cell or its organelles. Transcription factors, while searching for their binding sites, also experience 1D diffusion on DNA in addition to their 3D migration to different parts of the chromosome through cytosolic diffusion.[1,2] In all of these cases, the diffusion of single molecules is a random walk process and, thus biochemical reactions that involve these molecules represent a stochastic process.

Stochastic effects of diffusion are important for biological function, and have been considered in a number of contexts. For example, pioneering work from Berg and Purcell[3] analyzed the effects of diffusion and reaction-diffusion processes for a host of different biological scenarios, such as an evolutionary revealing back of the envelope calculation of the minimum number and size of absorbers required to efficiently internalize environmental nutrients into the cell (answer: small and not that many). They also calculated the approximate time required for a cell to measure the mean concentration, within a certain statistical confidence, of some external chemical that exhibits stochastic diffusion-driven concentration fluctuations. More recently, in the spirit of Berg and Purcell, more sophisticated diffusion-reaction approaches have been developed to estimate morphogen concentrations for patterning and development.[4]

The diffusion of molecules coupled to their involvement in chemical reactions can play a critical role in signal transduction. For example, receptors on the surface of a cell can homo- or hetero-dimerize in response to ligand stimulation, a process that is often instrumental in the subsequent transmission of environmental information to initiate downstream signaling. This process involves the interaction of receptors with ligands, their diffusion on the cell surface, and often their encounter and favorable collision for the formation of dimers or higher order oligomers. For example, diffusion-reactions of around 200 molecules of Ire1 on the elaborate endoplasmic reticulum membrane represent a crucial step in the triggering of the unfolded protein response in eukaryotes.[5] As a result, quantitative understanding of how membrane diffusion-reactions quantitatively contribute to the dynamic properties and variability of biochemical reactions is crucial for accurate and predictive mathematical modeling of such systems.

The stochastic theory of diffusion-reactions is a rich theory. As early as 1917, stochastic waiting time equations for the probability of a diffusing molecule to react with another molecule in solution was derived by Smoluchowski.[6] This early work illustrated that, in general, the waiting time for the reaction to occur does not necessarily follow an exponential distribution. Building upon Smoluchowski's work, Collins and Kimball[7,8] updated the theory to include partially reflecting boundaries on the reacting molecules. Others developed these ideas further by including force potentials with applications to fluorescence quenching.[9] In recent work, analytical results were derived for collision times between two molecules on a sphere when their dynamics are governed by stochastic differential equations.[10] These results were used to obtain general reaction rates, but did not involve

a)Electronic mail: Michael.Chevalier@ucsf.edu.
b)Electronic mail: Hana.El-Samad@ucsf.edu.
c)URL: http://biochemistry.ucsf.edu/labs/elsamad/home/index.html.

any assessment of the spatial distribution of molecules generated by stochastic effects. Many algorithmic developments, based on Smoluchowski's work and related work by Kim and Shin[11] tackled efficient implementations of general Brownian dynamics (BD),[12–14] among these is a recent technique known as Green's function reaction dynamics (GFRD) (Ref. 14) which propagates the Brownian dynamics of molecules starting from an initial δ function in space instead of a uniform distribution. Overall, these studies brought forward the idea that accounting for diffusion and geometry is important and that ignoring such effects is prone to artifacts generated by the usually held assumption that interactions between biological molecules occur in a well-stirred, three-dimensional environment.

In contrast to BD where every molecule and its spatial position is tracked, many investigations of stochastic biochemically reacting systems rely on the stochastic simulation algorithm (SSA) developed by Gillespie.[15] In the framework of the SSA, which assumes well-mixing, the behavior of the biological molecules follows a continuous-time discrete state Markov process, implying that the time-dependent probabilities for molecules to react are described by a single decaying exponential. As a result, neither individual molecules nor their coordinates need to be accounted for, allowing for only the molecular numbers of a given reaction species to be tracked. In a recent development, the SSA has been combined with spatial meshes to model reaction-diffusion systems in a form known as the reaction-diffusion master equation (RDME).[16,17] Here, space is divided into cells and reacting molecules can either react within a spatial cell based on SSA/Markov reaction assumptions (whose rates can scale with the mesh size[17]) or they can diffuse to different spatial cells. While, in many regimes, the RDME is typically orders of magnitude faster and as accurate as BD and GFRD, in cases where the spatial cell size becomes too coarse or too small relative to the molecular concentration and cellular geometry, the modeling of diffusion-limited bimolecular reactions becomes inaccurate.[18]

In this work, we draw attention to an intermediate regime that lies between the SSA and BD/GFRD/RDME simulations. Specifically, we derive an approximate formulation which allows us to capture the non-memoryless reaction time behavior of molecules diffusing on biological membranes without explicitly taking into account their spatial coordinates over time. This formulation relies on a hybrid numerical/analytical method to determine waiting time distributions for diffusion-reactions between two molecules diffusing in a few simple, but biologically relevant, geometrical settings. While the SSA makes the implicit assumption that waiting times between two molecules follow an exponential distribution, we illustrate that when diffusion of molecules is explicitly modeled, the analytical waiting time distributions are contribution of many exponentials (non-memoryless effects). We use these updated waiting time distributions to extend the SSA and test the new algorithm by benchmarking it against BD simulations in a few simple reacting systems on a sphere. For these cases, we show that accounting for memory effects arising from membrane diffusion and reactions is crucial and that doing so using the appropriate probability functions is an accurate and more computationally efficient alternative to tracking the molecules spatial coordinates. Our work advances the quantitative understanding of the role of space and membrane diffusion-reactions in biological systems, and provides a computationally tractable framework for probing these effects.

II. CALCULATION OF THE REACTION WAITING TIME DISTRIBUTION FOR A REACTING PAIR ON A 2D MEMBRANE

Our goal in this paper is to develop an algorithm that does not keep track of each reacting molecule's spatial coordinates, while still accounting for diffusion effects. We first develop probabilistic waiting time distributions for a diffusion-reaction to occur between two molecules then generalize these distributions to populations of reacting molecules and use those as basis for a stochastic simulation algorithm that extends the SSA.

Consider the two reacting molecules M_1 and M_2 on a 2D membrane (Figure 1(a)). We assume that the two reacting molecules, M_1 and M_2, have radii r_1 and r_2 and diffusion coefficients D_1 and D_2, respectively. In this work, we assume that $r_1 = r_2 = r_p$ and $D_1 = D_2 = D_p$. The molecules follow both translational and rotational diffusion with a rotational diffusion coefficient[19] given by $D_{rot} \approx D_p/(4r_p^2)$ rad^2 s^{-1}. In practice, biological molecules are not isotropic cylinders (2D) or spheres (3D), but have specifically located binding pockets. Therefore, we consider that the two molecules M_1 and M_2 have reacting surfaces that span an angle α_1 and α_2, respectively. When the molecules collide and the reacting surfaces align then a reaction occurs, otherwise, they reflect off of each other (Figure 1(a)).

One quantity is fundamental for quantifying the behavior of this two-molecule reacting system: $\widetilde{P}_{nr}(t)$, the probability that a reaction has not occurred by time t. Below, we derive the functional form of this probability while accounting for the diffusion of molecules. We will consider two scenarios. The first is the spatially uncorrelated case where the two molecules are placed randomly on the 2D membrane, randomly oriented with respect to each other, and then allowed to diffuse and react. The second case depicts a scenario in which a complex of two reacting molecules dissociates and these molecules are allowed to re-associate (spatially correlated pair). We then formulate an algorithm that uses $\widetilde{P}_{nr}(t)$ for the two scenarios to determine the reactions that occur between molecules and the time at which they occur. In the numerical examples, we show that the two distributions are sufficient to quantitatively describe many basic reacting systems seen in a biological context. In this fashion, using $\widetilde{P}_{nr}(t)$ incorporates the diffusion of molecules while circumventing the need to keep track of their exact spatial location.

A. Analytical framework for waiting time distributions

In this section, we set the framework for calculating $\widetilde{P}_{nr}(t)$ for two analytically tractable problems where molecules are undergoing diffusion-reaction on either a spherical membrane or a flat membrane (radially symmetric). We will show that as the number of reaction molecules increases

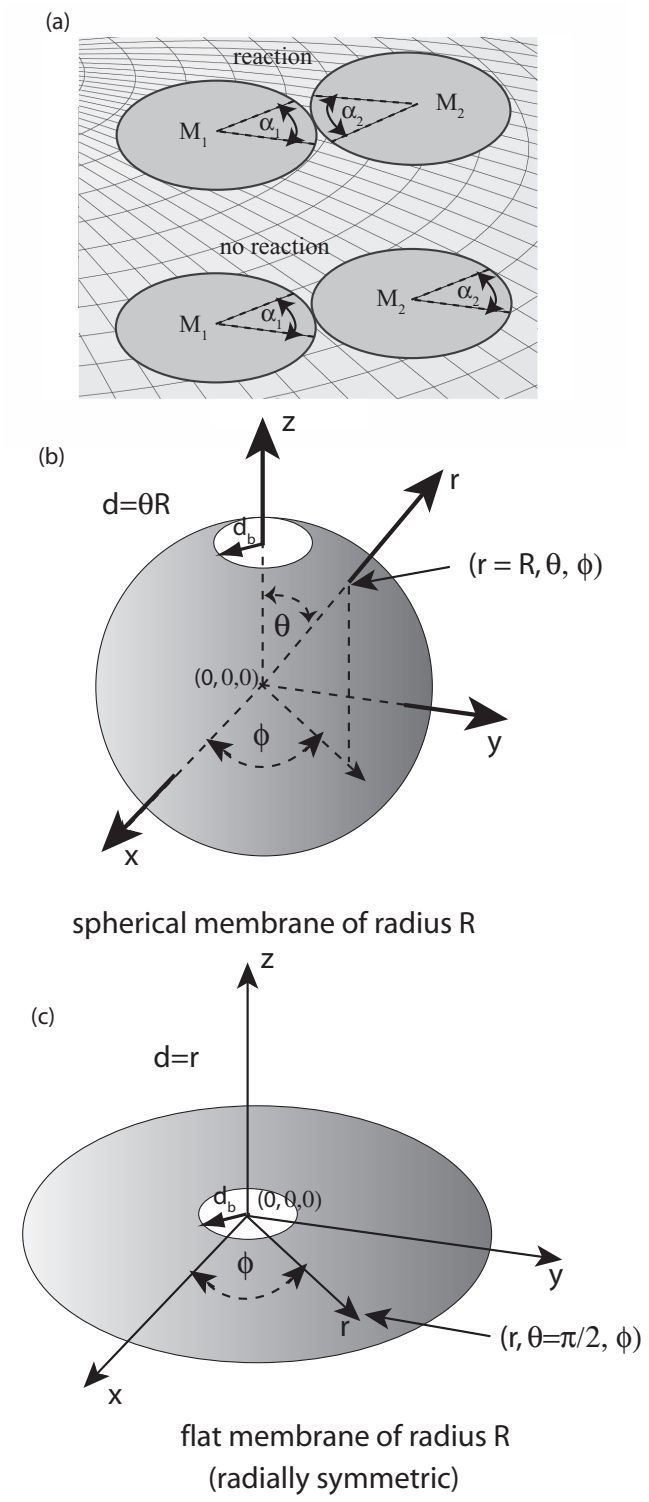

FIG. 1. Analytical approach for calculating reaction waiting time distributions. (a) Orientation-dependent reacting molecules: A schematic representation of how reactions can occur only when respective reacting surfaces collide. (b) Geometrical representation for analytical calculation of diffusion reaction system on a spherical membrane. (c) Geometrical representation for analytical calculation of diffusion reaction system on a flat membrane.

from two molecules (one M_1 and one M_2) to higher numbers, the waiting time distributions for spherical and flat membranes converge.

To begin, we setup the problem in the reference frame of one of the molecular species, for example M_1. If $d_b = r_1 + r_2$ is the sum of the two radii of the reacting molecules, the location of M_1 is modeled as a boundary condition (BC) at $d = d_b$. For the spherical membrane case, the boundary condition at $d = d_b$ is on the north pole of a sphere of radius R (Figure 1(b)). The distance variable is $d = \theta R$ where θ is the traditional angle from the z axis in spherical coordinates and where the outer distance is at $d_0 = \pi R$ (south pole). We are assuming azimuthal symmetry about the z axis since reactions can equally occur from any direction. Likewise for the 2D flat membrane case, the M_1 boundary condition is in the center at $d = d_b$ and the outer boundary distance is at $d_0 = R$ (Figure 1(c)).

In this formulation, the relative location of M_2 will be represented by a probability distribution in the remaining space of the 2D volume V (spherical membrane: $V = 4\pi R^2 - \pi d_b^2$, flat membrane: $V = \pi[R^2 - d_b^2]$). We define $p_2(d, t)$ as the probability density of finding M_2 at distance d at time t. The dynamics of $p_2(d, t)$ are governed by the diffusion equation

$$\frac{1}{D_r}\frac{\partial p_2(d,t)}{\partial t} = \nabla^2 p_2(d,t), \tag{1}$$

where $D_r = D_1 + D_2$ is the sum of the two molecules diffusion coefficients. The boundary condition at $d = d_b$ (that of M_1) will be a 2D partially reacting boundary condition[7,8,17] given by $2\pi d_b D_r \frac{\partial p_2(d=d_b,t)}{\partial d} - k p_2(d = d_b, t) = 0$ where k is the microscopic rate constant (rad μm^2 s^{-1} (2D)). For molecules used in this paper, k will depend on the reacting surface angles, α_1 and α_2 (Figure 1(a)), molecular radii, and the rotational diffusion coefficient. For every value of these problem-dependent variables, we can compute a unique k to use in the boundary condition (see Appendix B for method to fit k using a combination of BD simulations and the analytical approach described in this section). At $d = d_0$, the reflecting boundary condition is given by $\frac{\partial p_2(d=d_0,t)}{\partial d} = 0$. Therefore, probability is only absorbed at $d = d_b$ where the total probability in the space is decreasing over time.

Equation (1) can be solved using the separation of variables technique[20] which proceeds by decomposing the solution into orthogonal eigenfunctions. The solution is given by

$$p_2(d,t) = \sum_n A_n S_n(d) \exp(-D_r \kappa_n [t - t_s]). \tag{2}$$

The time $t = t_s$ represents the starting time of the analytical solution and $S_n(d)\exp(-D_r\kappa_n[t - t_s])$ is the nth eigenfunction with amplitude A_n. For the spherical membrane case, $S_n(d)$ are Legendre polynomials of the first kind of order $m = 0$ and degree ν_n. For the flat membrane case, the spatial functions are linear combinations of cylindrical bessel functions of the first and second kind. The boundary conditions for each spatial eigenfunction must also be $2\pi d_b D_r \frac{\partial S_n(d=d_b)}{\partial d} - k S_n(d = d_b) = 0$, $\frac{\partial S_n(d=d_o)}{\partial d} = 0$, as was the case for the total solution $p_2(d,t)$. Given the particular boundary conditions, it is easy to setup the transcendental equation to numerically solve for the eigenvalues by applying existing toolboxes and algorithms.[21–23]

The expression for each eigenfunction amplitude coefficient A_n is obtained from the initial distribution at the starting

time $t = t_s$:

$$A_n = \frac{\int_V p_2(d, t_s) S_n(d) dV}{\int_V S_n^2(d) dV}. \quad (3)$$

At any time t, for $t \geq t_s$, the sum of the probability that has either been absorbed or that remains in the space must add up to the initial probability at time t_s

$$\int_V p_2(d, t) dV + \int_{t_s}^{t} D_r \frac{\partial p_2(d, t')}{\partial d} \sigma dt' = \int_V p_2(d, t_s) dV = \widetilde{P}_{nr}(t_s), \quad (4)$$

where σ is the surface area of the molecule ($\sigma = 2\pi d_b$ (2D)). Consequently, the probability that no reaction has occurred by time t is given by

$$\widetilde{P}_{nr}(t) = \int_V p_2(d, t) dV = \widetilde{P}_{nr}(t_s) - \int_{t_s}^{t} D_r \frac{\partial p_2(d, t')}{\partial d} \sigma dt'. \quad (5)$$

$\widetilde{P}_{nr}(t)$ can be expressed as

$$\widetilde{P}_{nr}(t) = \exp(-\log(\widetilde{P}_{nr}(t))) = \widetilde{P}_{nr}(t_s) \exp\left(-\int_{t_s}^{t} \widetilde{a}(t') dt'\right). \quad (6)$$

Here $\widetilde{a}(t')$ can be seen as the time dependent reaction propensity for the bimolecular reaction between the two molecules. In general $\widetilde{P}_{nr}(t)$, although monotonically decreasing, is not a single exponential and hence, $\widetilde{a}(t')$ must be time-dependent.

B. Waiting time distribution for the spatially uncorrelated case

For the spatially uncorrelated case, we start with $t_s = 0$ and assume a uniform initial distribution of the molecules given by $p_2(d, t_s) = 1/V$ (Figure 2(a)). In this case, $\widetilde{P}_{nr}(t = 0) = 1$. The coefficients A_n are then determined from (3). We will represent this distribution as $\widetilde{P}^u_{nr}(t)$ where the u denotes uncorrelated.

Now, for a given surface area, we analyze the differences between the resulting $\widetilde{P}^u_{nr}(t)$ for the spherical membrane and the flat membrane cases using $d_b = 0.056\ \mu$m, $D_r = 2\ \mu$m^2/s, both biologically realistic values for protein diameters and membrane diffusion constants,[5] and $k = \infty$ (implying that $\alpha_1 = \alpha_2 = 360$). For the spherical membrane case, $R/d_b = 100$, and for an equivalent surface area in the flat membrane case, $R/d_b = 200$. For the spherical membrane case, at distances $d \ll \pi R$ near d_b the local surface is relatively flat, therefore the two approaches should yield very similar solutions over these distances and corresponding timescales. Indeed, the solutions overlap very well (Figure 2(b)) for $t < 0.03$ s where 0.025 of the probability has decayed, and slightly diverge over the remaining time in the plot. The differences at the later times are due to curvature.

If a given M_1 molecule has N_2 potential M_2 reacting partners each of which are spatially uncorrelated at time $t = 0$, then the probability for a reaction not to occur is simply $[\widetilde{P}^u_{nr}(t)]^{N_2}$. In Figure 2(c), we plot $[\widetilde{P}^u_{nr}(t)]^{N_2}$ for $N_2 = 50$ and $N_2 = 100$ for $t < 0.03$. The curves agree quite well for the two geometrical approaches implying that for larger population sizes curvature does not play a big part nor due to differences in the outer spatial boundaries between the two geometrical approaches. Clearly the curves are not single exponentials. An exponential function was fit to $[\widetilde{P}^u_{nr}(t)]^{N_2}$ for $N_2 = 100$, intersecting the true solution at approximately the $1/e$ value. However, if the same exponential is re-scaled for the $N_2 = 50$ case, then it undershoots the correct solution

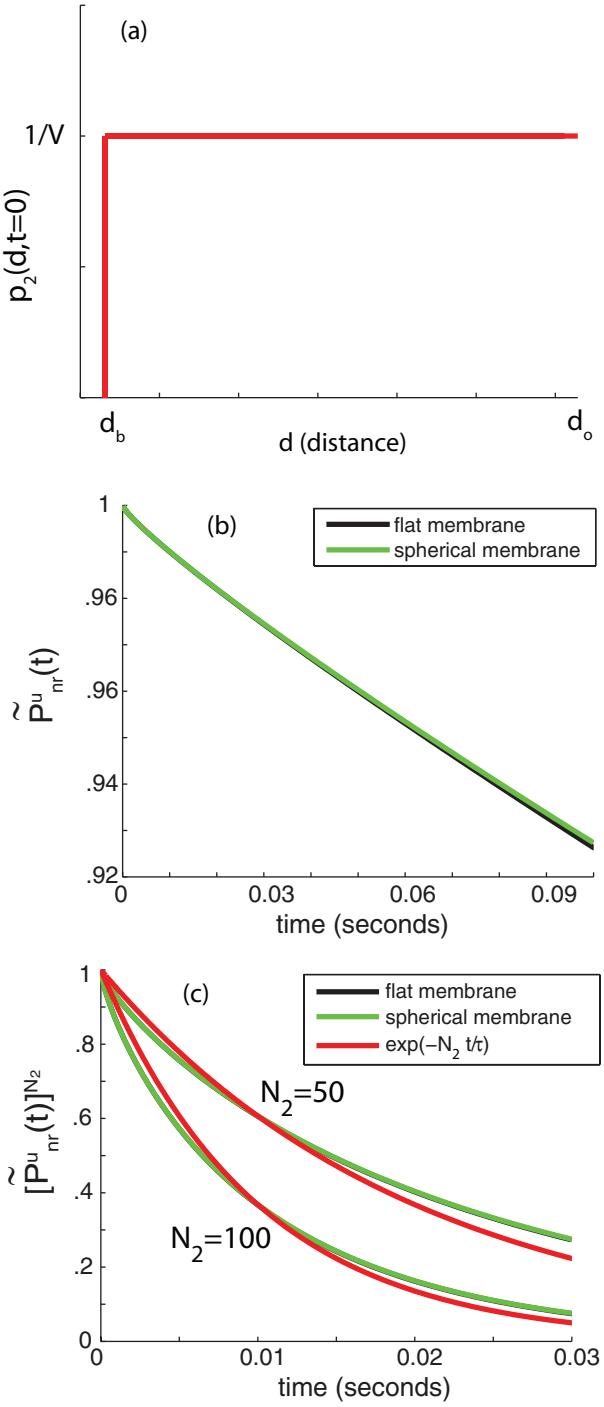

FIG. 2. Results for the spatially uncorrelated case. (a) initial conditions: $p_2(d, t = 0) = 1/V$. (b) $\widetilde{P}_{nr}(t)$ analytical solution ($k = \infty$). (c) $(\widetilde{P}_{nr}(t))^{N_2}$ analytical solution ($k = \infty$) vs fitted exponential for $N_2 = 50$ and 100.

(Figure 2(c)). This indicates that $[\widetilde{P}^u_{nr}(t)]^{N_2}$ contains the sum of multiple exponential terms. In Appendix C, we further analyze the eigenfunction solution and show that while for membranes (2D), $\widetilde{P}^u_{nr}(t)$ is always non-memoryless, 3D (diffusion reactions within the cytosol) systems approach the memoryless regime much faster.

C. Brownian dynamics/analytical approach to determine reassociation (correlated) waiting time distribution

We now assume that molecules are not uniformly positioned with respect to each other. Our aim here is to capture the correct reaction statistics at time $t > 0$ for a complex of two isotropic molecules M_1 and M_2 that has dissociated at time $t = 0$. We would like to calculate $\widetilde{P}^c_{nr}(t)$, the probability for the molecules M_1 and M_2 not to re-associate. For this paper, we will assume that when M_1 and M_2 dissociate, they are separated by an initial distance $d_r = .3r_p + d_b$ and that their relative orientation $\Delta\phi_r$ is correlated but with some randomness, in this case, $-\frac{\pi}{2} \leq \Delta\phi_r \leq \frac{\pi}{2}$ (Figure 3(a)). The particular value of d_r used in this paper represents a biologically realistic unbinding radius value.[12] In general, the initial distance d_r could also be a random variable. Note that if we compute this problem in the reference frame of molecule M_1, then it is radially symmetric in the xy plane (Figure 3(a)). That is, all we need to do is rotate the molecule M_2, azimuthally about M_1 (orientation of M_1 rotates accordingly) at the fixed distance d_r. When the two molecules become uncorrelated at some time t_s, we can connect the results of BD to the analytical solution described in Sec. II (with the microscopic reaction rate k already fitted for the reaction pair). It is important to note that we cannot apply the analytical model at $t = 0$ since the molecule orientations are partially correlated. However, we can revert back to the analytical results at some time $t = t_s$ when the orientations become uncorrelated (as a rule of thumb, because we use a finite number of modes in our analytical series solutions, t_s cannot be smaller than timescale of the fastest mode calculated). Therefore, the waiting time distribution $\widetilde{P}^c_{nr}(t)$ will be a pasted solution comprised of the BD results for $t \leq t_s$ and the analytical continuation results for $t > t_s$.

To compute $\widetilde{P}^c_{nr}(t)$, we use BD simulations starting with the reacting molecules M_1 and M_2 a fixed distance d_r apart and sample their relative orientation from the distribution of the random variable $\Delta\phi_r$. Next, given diffusion coefficient values, we apply both translation and rotational random walks and record the relative distance between the molecules over time until the two molecules react (or until some maximum time is reached). We repeat the process for a large number of trials and compute $C_2(d, t = t_s) = \int_{d_b}^{d} p_2(d', t = t_s)dV'$, the fraction of trial instances where the M_2 molecule is between $d_b \leq d' \leq d$ at time t_s (Figure 3(b)). This is done for a number of sample values of d. $C_2(d, t = t_s)$ can then be approximated using a third order spline fitting procedure (Figure 3(b), green curve), and then differentiated to yield an approximate $p_2(d, t = t_s)$, $\tilde{p}_2(d, t = t_s)$ (Figure 3(c)). The function $\tilde{p}_2(d, t = t_s)$ is used in Eq. (3) to obtain the eigenfunction amplitudes, A_n. This allows us to compute $\widetilde{P}^c_{nr}(t)$ analytically for $t \geq t_s$. Figure 3(d) shows the BD and analytical continuation results for $R/d_b = 100$, $\alpha = 60$, and $k = 1.30$. Here one immediately notices that $\widetilde{P}^c_{nr}(t)$ has many timescales and therefore corresponds to a non-memoryless system. In the next section, we combine $\widetilde{P}^u_{nr}(t)$ and $\widetilde{P}^c_{nr}(t)$ to form a general stochastic simulation algorithm.

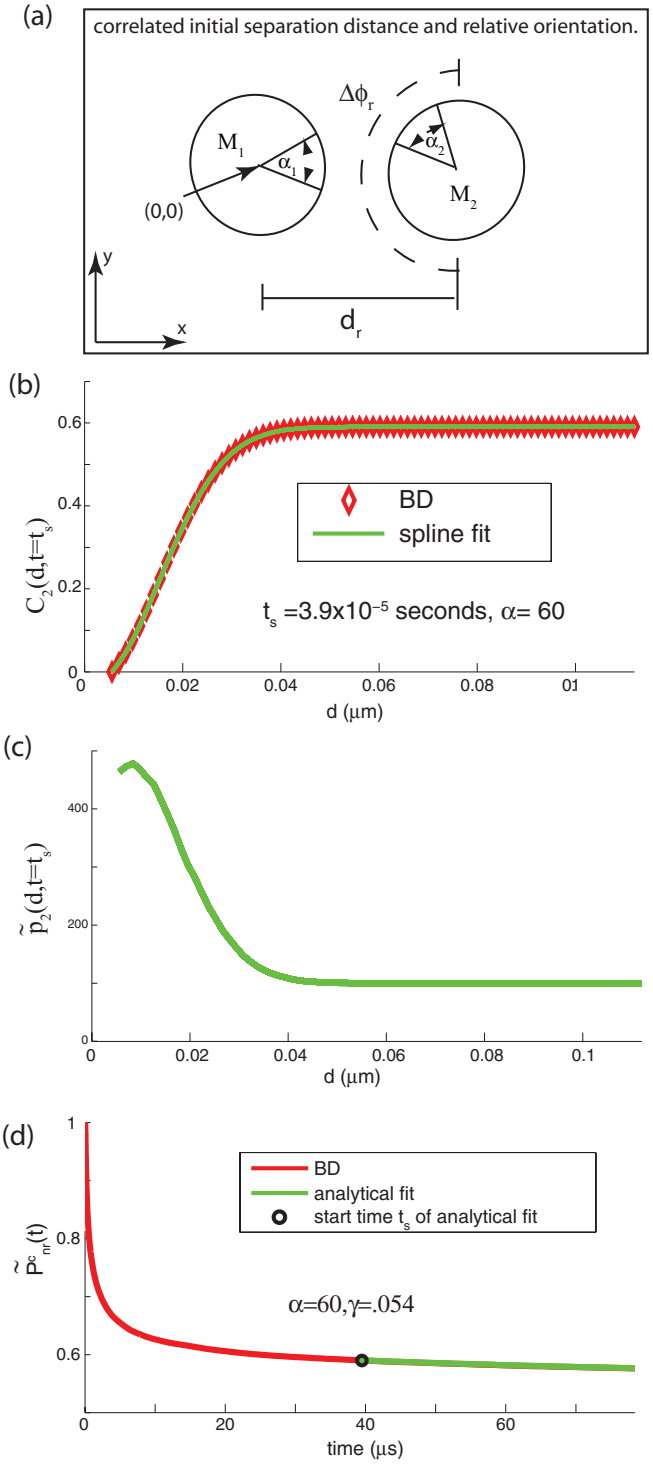

FIG. 3. Analytical/BD approaches for fitting $\widetilde{P}^c_{nr}(t)$: (a) Initial conditions. (b) $C_2(d, t = t_s)$ at time $t = t_s$ where $t_s = 3.9 \times 10^{-5}$ and $\alpha = 60$, $k = 1.30$. (c) Spline fitted function $\tilde{p}_2(d, t = t_s)$. (d) Pasted solution $\widetilde{P}^c_{nr}(t)$ of BD results and analytical continuation.

III. NON-MEMORYLESS STOCHASTIC SIMULATION ALGORITHM USING $\widetilde{P}^u_{nr}(t)$ AND $\widetilde{P}^c_{nr}(t)$

With $\widetilde{P}^u_{nr}(t)$ and $\widetilde{P}^c_{nr}(t)$ at hand, we can formulate a simple Monte Carlo simulation algorithm that approximates membrane diffusion-reaction systems without explicitly tracking the spatial locations of molecules. Here reaction times are generated using $\widetilde{P}^u_{nr}(t)$ and $\widetilde{P}^c_{nr}(t)$ to determine the reactions that occur in the system and their time of occurrence. Viewed in this light, this constitutes an updated form of the stochastic simulation algorithm (SSA), a routinely used procedure for the simulation of biochemically reacting molecules in a well-stirred environment.[15] The SSA assumes that the reactions are well-described by a continuous-time discrete state Markov process. As a result, $\widetilde{P}_{nr}(t)$ always takes the form of a single decaying exponential, which is then used to determine numerically what reactions occur in the system and the time at which they occur. Therefore, our new algorithm proceeds in the same spirit as the SSA, but bases computations on $\widetilde{P}^c_{nr}(t)$ and $\widetilde{P}^u_{nr}(t)$. Two simple general rules are needed to complete the specification of the algorithm:

1. Dissociated pairs that have not yet reacted are correlated to each other ($\widetilde{P}^c_{nr}(t)$) while all other reacting molecules are spatially uncorrelated ($\widetilde{P}^u_{nr}(t)$) with respect to the pair.
2. A newly created molecule sees all other reacting molecules as spatially uncorrelated ($\widetilde{P}^u_{nr}(t)$).

Keep in mind that we are only keeping track of correlated pairs and any third molecule (and higher) correlations are ignored.

For the spatially uncorrelated diffusion-reactions, the probabilistic waiting time for a reaction to occur between the ith molecule of type m and the jth molecule of type n, $\widetilde{P}^u_{nr}(t-\max(t_{m_i},t_{n_j}))$ (in a homo-dimerization case type m is the same as type n), has the basic form

$$\widetilde{P}^u_{nr}(t-\max(t_{m_i},t_{n_j})) = \exp\left(-\int_{\max(t_{m_i},t_{n_j})}^{t}\widetilde{a}_u(t'-\max(t_{m_i},t_{n_j}))dt'\right). \quad (7)$$

The times t_{m_i} and t_{n_j} are the molecules respective creation times and $\max(t_{m_i},t_{n_j})$ dictates that the interaction can only occur after the last molecule of the reaction pair is created. Given any $\tau \geq \max(t_{m_i},t_{n_j})$ and molecules m_i and n_j which have not yet reacted by time τ,

$$\begin{aligned}\widetilde{P}^u_{nr}(t-\max(t_{m_i},t_{n_j})|\tau) &= \frac{\widetilde{P}^u_{nr}(t-\max(t_{m_i},t_{n_j}))}{\widetilde{P}^u_{nr}(\tau-\max(t_{m_i},t_{n_j}))}\\ &= \exp\left(-\int_{\tau}^{t}\widetilde{a}_u(t'-\max(t_{m_i},t_{n_j}))dt'\right),\end{aligned} \quad (8)$$

for $t>\tau$. $\widetilde{P}_{nr}(t-\max(t_{m_i},t_{n_j})|\tau)$ fundamentally depends on the creation time $\max(t_{m_i},t_{n_j})$, and is therefore a function of the history prior to time τ as long as $\widetilde{a}(t'-\max(t_{m_i},t_{n_j}))$ is not a constant. The same logic holds for $\widetilde{P}^c_{nr}(t-\max(t_{m_i},t_{n_j}))$ where

$$\widetilde{P}^c_{nr}(t-\max(t_{m_i},t_{n_j})|\tau) = \exp\left(-\int_{\tau}^{t}\widetilde{a}_c(t'-\max(t_{m_i},t_{n_j}))dt'\right). \quad (9)$$

Here, at the dissociation time, $t_{m_i}=t_{n_j}$. Therefore, the expression $\max(t_{m_i},t_{n_j})$ is still applicable. A simple mathematical transformation eases the implementation of the algorithm. We rewrite $\widetilde{P}^c_{nr}(t-\max(t_{m_i},t_{n_j})|\tau)$ as

$$\begin{aligned}&\widetilde{P}^c_{nr}(t-\max(t_{m_i},t_{n_j})|\tau)\\ &= \widetilde{P}^u_{nr}(t-\max(t_{m_i},t_{n_j})|\tau)\frac{\widetilde{P}^c_{nr}(t-\max(t_{m_i},t_{n_j})|\tau)}{\widetilde{P}^u_{nr}(t-\max(t_{m_i},t_{n_j})|\tau)}\\ &= \widetilde{P}^u_{nr}(t-\max(t_{m_i},t_{n_j})|\tau)\widetilde{P}^{mc}_{nr}(t-\max(t_{m_i},t_{n_j})|\tau)\\ &= \exp\left(-\int_{\tau}^{t}\widetilde{a}_u(t'-\max(t_{m_i},t_{n_j}))dt'\right)\\ &\quad\times\exp\left(-\int_{\tau}^{t}\widetilde{a}_{mc}(t'-\max(t_{m_i},t_{n_j}))dt'\right).\end{aligned} \quad (10)$$

Equation (10) states that the correlated pair can react through a spatially uncorrelated interaction $\widetilde{P}^u_{nr}(t-\max(t_{m_i},t_{n_j})|\tau)$ and a modified correlated interaction $\widetilde{P}^{mc}_{nr}(t-\max(t_{m_i},t_{n_j})|\tau)$. Therefore, every pair of molecules can react through a spatially uncorrelated interaction, and if a given pair is also correlated, then the molecules also react through the modified correlated interaction.

One of the standard functions in the SSA is the cumulative distribution function $P_{nr}(t|\tau)$ which describes the probability that any type of reaction has not occurred by time t, given that no reaction has occurred by τ for $t\geq\tau$. The stochastic occurrence of a reaction is assumed to be independent of all other reactions and therefore $P_{nr}(t|\tau)$ is the product of the "probability of no reaction" functions for every reaction.

Given a system consisting of $M+2$ reactions, with M memoryless reactions, one spatially uncorrelated diffusion-reaction (reaction number $M+1$), and one spatially correlated diffusion-reaction (reaction number $M+2$), $P_{nr}(t|\tau)$ can be expressed as

$$\begin{aligned}&P_{nr}(t|\tau)\\ &= \exp\left(-\sum_{j=1}^{M}a_j(x)[t-\tau]\right)\\ &\quad\times\exp\left(-\sum_{i,j}\int_{\tau}^{t}\widetilde{a}_u(t'-\max(t_{m_i},t_{n_j}))dt'\right)\\ &\quad\times\exp\left(-\sum_{k}\int_{\tau}^{t}\widetilde{a}_{mc}(t'-\max(t_{m_{i(k)}},t_{n_{j(k)}}))dt'\right).\end{aligned} \quad (11)$$

The first term on the right side of the equations represents the waiting time distributions for the M memoryless reactions. In

this term, x is the current state of the system and the functions $a_j(x)$ are the propensities of the memoryless reactions. The second term represents the product of all the individual spatially uncorrelated diffusion-reaction waiting time distributions. Finally, the third term represents the product of all the individual modified-correlation diffusion-reaction waiting time distributions (where k is the index of the kth correlated pair). The spatially uncorrelated interactions counts through every reaction pair and the modified correlated interaction counts through only the correlated pairs. The cumulative distribution function that a reaction has occurred by t, given that no reaction has occurred by τ is given by $P_r(t|\tau) = 1 - P_{nr}(t|\tau)$. Therefore, the conditional time dependent probability density function (pdf) for a reaction to occur is given by

$$\begin{aligned} p_r(t|\tau) &= -\frac{\partial P_{nr}(t|\tau)}{\partial t} \\ &= [A_m + A_u + A_{mc}]P_{nr}(t|\tau), \end{aligned} \tag{12}$$

where $A_m = \sum_{j=1}^{M} a_j(x)$, $A_u = \sum_{i,j} \widetilde{a}_u(t - \max(t_{m_i}, t_{n_j}))$, and $A_{mc} = \sum_k \widetilde{a}_{mc}(t - \max(t_{m_{i(k)}}, t_{n_{j(k)}}))$. The final function needed is $p(\mu, t|\tau)$, the joint probability density function for a reaction of type μ to occur at time t. It can be expressed as $p(\mu, t|\tau) = p_r(t|\tau)p(\mu|t, \tau)$. For $\mu \leq M$, the function $p(\mu|t, \tau)$ is expressed as

$$\begin{aligned} p(\mu, t|\tau) &= [A_m + A_u + A_{mc}]P_{nr}(t|\tau) \\ &\quad \times \frac{a_\mu(x)}{[A_m + A_u + A_{mc}]} \end{aligned} \tag{13}$$

and for $\mu = M + 1$, it is expressed as

$$\begin{aligned} p(\mu, t|\tau) &= [A_m + A_u + A_{mc}]P_{nr}(t|\tau) \\ &\quad \times \frac{\sum_{i,j} \widetilde{a}(t - \max(t_{m_i}, t_{n_j}))}{[A_m + A_u + A_{mc}]}. \end{aligned} \tag{14}$$

A similar expression for the $\mu = M + 2$ (correlated pairs) is easily obtained.

With these functions at hand, we can formulate a simulation algorithm which, much like the SSA, proceeds by sampling the time and type of the next reaction from $p(\mu, t|\tau)$. This is done by first sampling the time of the next reaction from $p_r(t|\tau)$ and then sampling the type of reaction from $p(\mu|t, \tau)$. In addition to this basic framework, we need to sample the reacting molecule pair by defining the function $p(m_k, n_\ell|\mu = M + 1, t, \tau)$, the probability that, given the reaction time t, the spatially uncorrelated diffusion reaction that occurred was between molecules m_k and n_ℓ. It has the form

$$p(m_k, n_\ell|\mu = M + 1, t, \tau) = \frac{\widetilde{a}(t - \max(t_{m_i}, t_{n_\ell}))}{\sum_{i,j} \widetilde{a}(t - \max(t_{m_i}, t_{n_j}))}. \tag{15}$$

A similar expressions, if a correlated diffusion reaction occurs ($\mu = M + 2$) is easily obtained to determine the particular reaction pair. The algorithm proceeds as follows:

Algorithm:

Initialize system at $t = \tau = 0$. Initialize state x. For molecule types m and n, initialize molecule stacks, both spatially uncorrelated molecule stacks and the correlated pair molecule stack. Unless more complicated initial conditions are required, for simplicity, all creation times for the initial m and n type molecules are assumed to be at time zero, i.e., $t_{m_i} = 0$ for all i and $t_{n_j} = 0$ for all j. Go to 1.

1. **Determine time of next reaction, t_r:** Generate a random number λ_r from a uniform distribution between 0 and 1. Solve

$$\int_\tau^{t_r} p_r(t'|\tau)dt' = P_r(t_r|\tau) = \lambda_r.$$

2. **Sample the reaction from $p(\mu|t_r, \tau)$:** Generate a random number, λ_μ, from a uniform distribution between 0 and 1. Find μ that satisfies

$$\sum_{i=1}^{\mu} p(i|t_r, \tau) < \lambda_\mu \leq \sum_{i=1}^{\mu+1} p(i|t_r, \tau).$$

If $\mu = M + 1$, i.e., spatially uncorrelated diffusion-reaction, then go to 3. If $\mu = M + 2$, i.e., modified correlated diffusion-reaction, then go to 4. Otherwise go to 5.

3. **Spatially uncorrelated diffusion reaction pair:** Generate a random number, $\lambda_{k,\ell}$ from a uniform distribution between 0 and 1. Find the reaction pair, m_k, n_ℓ that satisfies

$$\begin{aligned} &\frac{\sum_{i,j}^{p(k,\ell)} \widetilde{a}_u(t - \max(t_{m_i}, t_{n_j}))}{\sum_{i,j} \widetilde{a}_u(t - \max(t_{m_i}, t_{n_j}))} \\ &< \lambda_{k,\ell} \leq \frac{\sum_{i,j}^{p(k,\ell)+1} \widetilde{a}_u(t - \max(t_{m_i}, t_{n_j}))}{\sum_{i,j} \widetilde{a}_u(t - \max(t_{m_i}, t_{n_j}))} \end{aligned}$$

where the counter variable $p(k, \ell)$ simply represents the 1D count mapping of the index counters k and ℓ. Remove the reacted molecules and readjust the m and n spatially uncorrelated molecule stacks. Also if either molecules are part of a correlated pair, remove from the correlated pair molecule stack as well. For all m molecules where $i > k$, set $i = i - 1$. Similarly, For all n molecules where $j > \ell$, set $j = j - 1$. Go to 6.

4. **Modified correlated diffusion reaction pair:** Generate a random number, λ_ℓ from a uniform distribution between 0 and 1. Find the reaction pair, $m_{i(\ell)}$, $n_{j(\ell)}$ (where ℓ is the index of the ℓth correlated pair), that satisfies

$$\begin{aligned} &\frac{\sum_{k}^{\ell} \widetilde{a}_{mc}(t - \max(t_{m_{i(k)}}, t_{n_{j(k)}}))}{\sum_{k} \widetilde{a}_{mc}(t - \max(t_{m_{i(k)}}, t_{n_{j(k)}}))} \\ &< \lambda_\ell \leq \frac{\sum_{l}^{\ell+1} \widetilde{a}_{mc}(t - \max(t_{m_{i(k)}}, t_{n_{j(k)}}))}{\sum_{k} \widetilde{a}_{mc}(t - \max(t_{m_{i(k)}}, t_{n_{j(k)}}))}. \end{aligned}$$

Remove the reacted molecules and readjust the m and n spatially uncorrelated molecule stacks and the correlated molecule pair stack. For all m molecules where $i > k$, set

$i = i - 1$. Similarly, For all n molecules where $j > \ell$, set $j = j - 1$. Go to 6.

5. **Memoryless reactions:** If molecule of type m or n is created then add to the respective molecule stack. If a molecule of type m or n is destroyed then randomly sample which molecule is destroyed (all molecules in the spatially uncorrelated molecule stacks are equally likely) and adjust the spatially uncorrelated molecule stacks and the correlated pair stack accordingly. If the reaction is a dissociation with a resulting correlated pair, then add to the correlated pair stack. Go to 6.
6. **Adjust the state** $x = x + \nu_\mu$: Set $t = \tau = t_r$. Go to 1.

Because the algorithm is a generalization of the original SSA, we name it the non-memoryless stochastic simulation algorithm (NMSSA).

IV. SIMPLE DIFFUSION REACTION SYSTEMS ON A SPHERE

We apply the NMSSA algorithm to a few simple, biologically relevant, diffuion-reactions systems on the surface of a sphere. To assess the accuracy of the NMSSA algorithm, we compare its results to full BD simulations where all time-dependent positions, diffusive transport, and collisions between molecules and reactions are accounted for (see Appendix A for full details of algorithm and implementation).

For all the results reported below, simulations were run until a total of >200 000 diffusion reactions occurred. Stationary distributions were obtained from these time traces.

In all BD simulations, molecules have a radius of $r_1 = r_2 = .0028$ μm and a diffusion coefficient $D_p = 1.0$ $\mu m^2/s$. We only assume spherical geometries of radius R with $R/d_b = 100$ (unless otherwise noted), where $d_b = r_1 + r_2$ is the sum of the two reacting radii. The updated time steps is $\Delta t = 3.4 \times 10^{-9}$, small enough to accurately capture the stochastic dynamics for the molecules sizes r_p and the diffusion coefficient D_p.[16] $R/d_b = 100$ is chosen because of the quadratic nature of spatial dimensions vs. time in simulating diffusion, where systems with larger R/d_b become prohibitively expensive to simulate with the BD algorithm.

For the results presented, we assume that $\alpha_1 = \alpha_2 = \alpha$ and analyze molecules with binding angles $\alpha = 360$, 180, 120, and 60. Applying the fitting algorithm of Appendix B results in values of the boundary condition parameter $k = \infty$, 9.77, 3.85, and 1.30, respectively. These values were then used to calculate $\widetilde{P}^u_{nr}(t)$ and $\widetilde{P}^c_{nr}(t)$ as needed for each α.

A. Absorber system

The first basic system analyzed is given by the chemical equations

$$M_1 + M_2 \rightarrow \emptyset + M_2, \tag{16a}$$

$$\emptyset \rightarrow M_1, \tag{16b}$$

$$\emptyset \rightarrow M_2 \rightarrow \emptyset. \tag{16c}$$

The molecules M_1 are created at a rate β_{m_1} (mol s^{-1}). The M_2 are created and removed at constant rates, β_{m_2} (mol s^{-1}) and γ_{m_2} (s^{-1}), respectively. The diffusion-reaction of M_1 with M_2 results in the destruction of M_1 while M_2 itself remains unaffected. We refer to this set of biochemical reactions as the "absorber" system. In a biological context, absorber-like reactions model the binding of receptors to clathrin-coated-pits, resulting in their endocytosis.[24]

1. Non-memoryless effect of spatially uncorrelated reactions

To allow for direct comparison with analytical results, we first considered the case where the number of M_2 absorbers is constant and set to a value N_2, i.e., there is no source or sink in (16c).

For case 1, we set $\alpha = 360$, $\beta_{m_1} = \beta = 5 \times 10^4$, and $N_2 = 450$, and confirm that BD and NMSSA give quantitatively identical stationary distributions for M_1 (Figure 4(a), green and black dashed lines). Using the BD or NMSSA distribution, we can determine the mean of the M_1 distribution to be $\bar{M}_1 \approx 90$. If this system were memoryless, then the mean of the M_1 stationary distribution will be described by the equation:

$$\beta_{m_1} - k_{12}\bar{M}_1 N_2 = 0, \tag{17}$$

k_{12} would be the empirical reaction rate between M_1 and M_2. We can then use Eq. (17) and the BD simulation to extract a value for k_{12}. With this fitted value for k_{12}, we run SSA simulations (Figure 4(a), red line) which generate a distribution for M_1 that agrees well with the NMSSA for these parameter values. Now, if we choose the parameters to be

- Case 2: $\beta_{m_1} = 2\beta$, $N_2 = 900$
- Case 3: $\beta_{m_1} = \beta/9$, $N_2 = 50$

then the memoryless system description (Eq. (17)) predicts that the value of $\bar{M}_1 = \frac{\beta_{m_1}}{k_{12}N_2}$ should not change from the case 1 results. Stationary distributions obtained from SSA simulations for the three cases verify this prediction (Figure 4(a)). By contrast, the BD and NMSSA simulations show a lower mean than the SSA runs for case 2 and a higher mean for case 3 (Figure 4(a)). This again reiterates the fact that $\widetilde{P}^u_{nr}(t)$ features many exponentials that contribute to the solution and thus there is no fundamental rate constant k_{12} in the mass-action sense (these results concur with observations in other 2D systems[17]).

One feature of the BD and NMSSA distributions for case 3 (Figure 4(a), $N_2 = 50$) is that while their means coincide, the distribution width is wider in the BD simulation than for NMSSA. By contrast, for cases 1 and 2 where the number of N_2 molecules is much larger, BD and NMSSA agree well. The difference in distribution width in case 3 is likely the result of time-dependent spatial fluctuations at lower N_2 which are accounted for accurately in BD, but are averaged in the NMSSA. Recall that the functions $[\widetilde{P}^u_{nr}(t)]^{N_2}$ in Figure 4(a) should agree exactly between BD and NMSSA for all cases (only case 2 is shown) because they are calculated from all M_1 waiting times for a large number of BD simulations. However,

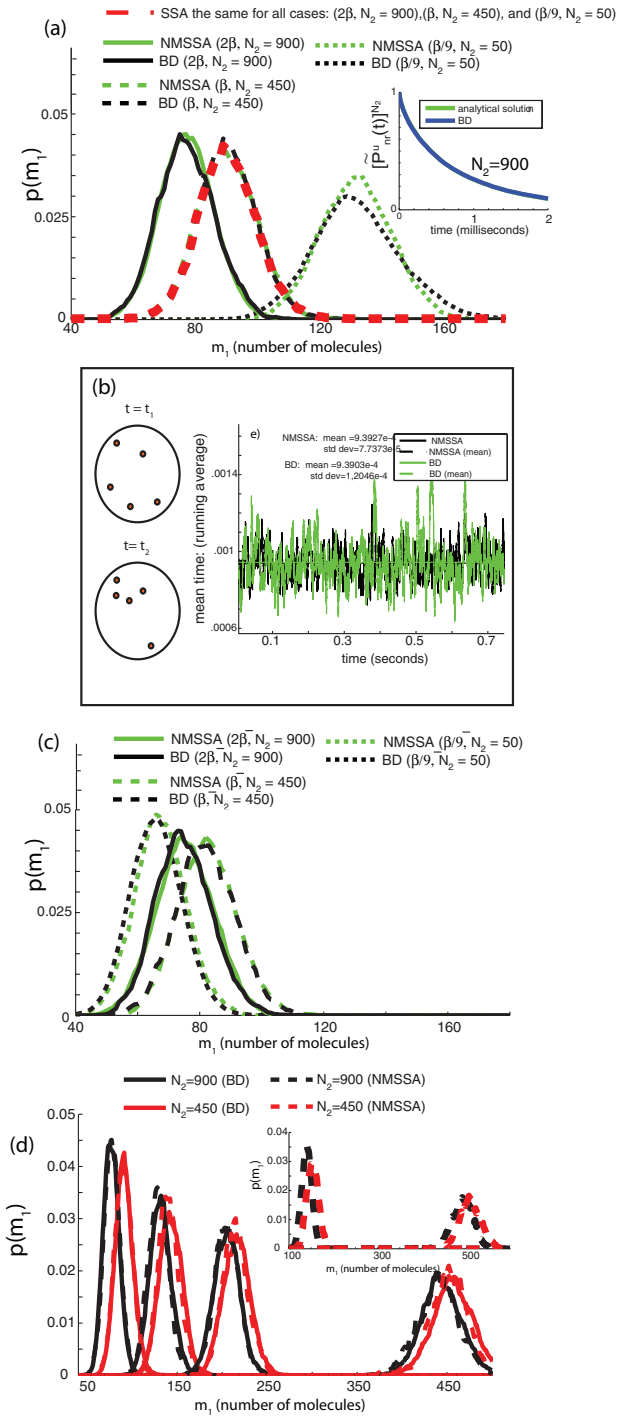

FIG. 4. Absorber system. (a) Stationary distributions ($\alpha = 360$) of M_1 for cases 1, 2, and 3. Inset is $[\widetilde{P}_{nr}(\tau)]^{N_2}$ for $N_2 = 900$. (b) Large spatial fluctuations have a high probability when low number of molecules are present. Right side: temporal variation in running average (200 points) of M_1 absorbing waiting times ($N_2 = 50$). (c) Stationary distributions ($\alpha = 360$) of M_1 for cases 1,2, and 3 when M_2 is stochastically synthesized and degraded. (d) Stationary distributions of M_1 for cases 1 and 2 (constant absorber scenario) and partially reflecting molecules of $\alpha = 360$, 180, 120, and 60 (left to right, respectively). Inset: Stationary distributions of M_1 for cases 1 and 2 (NMSSA only) for $R/d_b = 500$ and partially reflecting molecules for $\alpha = 360$ and 60 (left to right, respectively).

for NMSSA simulations, the function $\widetilde{P}^u_{nr}(t)$ is invariant over the entire simulation. That is, for a newly created M_1 molecule, the NMSSA draws from this invariant $\widetilde{P}^u_{nr}(t)$ distribution to calculate the absorbing waiting time. By contrast, for the BD simulations, a newly created M_1 molecule will see a specific spatial distribution of absorbers at a given time (Figure 4(b)). Its waiting time is thus influenced by this instantaneous spatial distribution. The BD simulation has, in essence, a time varying $\widetilde{P}_{nr}(t, S(\tau))$ whose variation is related to the time varying spatial fluctuations $S(t)$, while the NMSSA has at its disposal a static integral $\widetilde{P}^u_{nr}(t) = \frac{1}{T}\int_0^T \widetilde{P}_{nr}(t, S(\tau))d\tau$.

To illustrate this point, we compute the running average of the reaction waiting times for a sequence of M_1 molecules for both the BD and NMSSA simulation results. Since the BD simulations are influenced by the time-dependent fluctuations while the NMSSA simulations are not, larger fluctuations are observed for the BD simulations, exactly as expected (Figure 4(b), $\beta_{m_1} = \beta/9, N_2 = 50$, running window size of 200).

Next, we tested whether fluctuations in the number of M_2 molecules change the results by allowing for number fluctuations and a general spatial remixing of the M_2 population. To do so, we added probabilistic removal (sink, γ_{m_2}) and creation/placement (source, $\beta_{m_2} = 1 \times 10^5$) of M_2. In this case, the steady-state average of M_2 molecules is $\bar{N}_2 = \beta_{m_2}/\gamma_{m_2}$. The mean value was set to be $\bar{N}_2 = 450$ (case 1, $\gamma_{m_2} = 2.22 \times 10^2$), $\bar{N}_2 = 900$ (case 2,$\gamma_{m_2} = 1.11 \times 10^2$), and $\bar{N}_2 = 50$ (case 3,$\gamma_{m_2} = 2 \times 10^3$)). As above, we keep $\beta_{m_1}/\bar{N}_2$ constant to test deviation from the memoryless (exponential) assumption as these parameters change. In all cases, the BD and NMSSA simulations agree very well (Figure 4(c)). Notably, high absorber concentrations ($\bar{N}_2 = 900, 450$) generate distributions whose mean and width are similar to the constant absorber system.

In contrast, for $\bar{N}_2 = 50$, the mean of the distribution shifts below the means in case 1 and 2. Here, γ_{m_2} is an order of magnitude larger than for cases 1 and 2, leading to faster absorbing reaction times. This example demonstrates that the particular values used for β_{m_2} and γ_{m_2} in combination with $\widetilde{P}^u_{nr}(t)$ greatly affect the mean in the distributions as compared to the constant absorber case, and both the NMSSA and BD simulations capture this effect.

2. Orientation dependence of reactions facilitate convergence to memoryless behavior

Thus far, we have only analyzed isotropic molecules involved in reactions that are orientation independent. In practice, biological molecules on membranes are not isotropic identities, but rather complex molecules with 3D orientations and specifically located binding pockets. To reflect this, in addition to the $\alpha = 360$ case, cases 1 and 2 above were analyzed for $\alpha = 180$, 120, and 60 (Figure 4(d)) for the constant absorber number scenario. To quantify deviation from memoryless behavior, we calculated $\frac{\delta\mu}{\bar{\mu}}$, the normalized difference in means between the cases 1 and 2 stationary distributions for each value of α. For BD $\delta\mu/\bar{\mu}$ assumes the values $\delta\mu/\bar{\mu} \approx 0.17$ (360), 0.084 (180), 0.052, (120), and 0.024 (60). As expected, the same trends were measured for the NMSSA where $\delta\mu/\bar{\mu}$ assumed the values $\delta\mu/\bar{\mu} = 0.16$ (360), 0.087 (180), 0.048, (120), and 0.026 (60). The decrease

in $\delta\mu/\bar{\mu}$ indicated that the system became more memoryless as α decreases.

We then repeated the same tests for $R/d_b = 500$ and $\alpha = 360$ or 60. The values of β_{m_1} were reduced by a factor of 25 relative to the previous $R/d_b = 100$ simulations to yield similar distributions (Figure 4(d) inset). Here again, the non-memoryless behavior of the system dissipated as the binding angle was decreased ($\delta\mu/\bar{\mu} = 0.12$ (360) and 0.029 (60)). This observed convergence trend at lower α suggests that any condition on the molecules that decreases the rate of productive (reactive) collisions has the effect of re-stirring the system.

To frame these results in the context of the degree of diffusion control,[17] we define the diffusion control parameter to be $\beta = \frac{k}{2\pi D_r}$. β gauges how diffusion-limited versus rate-limited a given diffusion-reaction type is. For rate-limited reactions $\beta \ll 1$. For our system, $\beta = \infty$ ($\alpha = 360$), 0.78 ($\alpha = 180$), 0.31 ($\alpha = 120$), 0.1 ($\alpha = 60$). As expected, β is a decreasing function of α. However, even for molecules with $\alpha = 60$, there is still a reasonable degree of diffusion control. As α decreases towards zeros, it is expected that β converges to zero too. For these 2D rate-limiting cases the system will be memoryless and hence the memoryless SSA[15] would be applicable.

B. Reacting systems of homodimers and heterodimers at constant numbers

To test the NMSSA in a scenario where the effects of dissociation/reassociation of molecules become important, we considered a homo-dimerization reaction described by the chemical equation

$$M_1 + M_1 \rightleftharpoons M_2. \tag{18}$$

In these simulations, $\alpha = 60$ and the number of total molecules is held constant, $M_1 + 2M_2 = N_{tot}$. Biological systems often involve homo-dimerizing molecules, for example the oligomerization reaction of the receptor Ire1 molecule in the unfolded protein response.[5]

For a given total number of molecules, N_{tot}, the simulations were run for two different M_2 dissociation rates, $\gamma_d = 100$ and 1000. Three different values of N_{tot} were tested, $N_{tot} = 500$, 1000, and 1500 and the results plotted in Figure 5(a) ($\gamma_d = 100$) and Figure 5(b) ($\gamma_d = 1000$). In all cases, the NMSSA and BD results agree very well. To emphasize the necessity of applying the correlated distribution $\widetilde{P}^c_{nr}(t)$, we reanalyzed the system using the NMSSA but without accounting for correlation of molecules upon their dissociation. Instead, we assumed that upon dissociation, a given pair returns instantaneously to a spatially uncorrelated configuration. The results (dotted curves in Figures 5(a) and 5(b)) show a large error in the distributions for all cases.

We next considered a heterodimer system described by the chemical equation

$$M_1 + M_2 \rightleftharpoons M_3. \tag{19}$$

Three different values of $N_{tot} = 300$, 600, and 900 and two values of the M_3 dissociation rate ($\gamma_d = 100$ and 1000) were simulated. Again, the NMSSA and BD algorithms showed excellent agreement (Figures 5(c) and 5(d)) while ignoring spatial correlations generates the wrong solution. The results for the homodimer and heterodimer emphasizes the need to account for correlated reactions, but also illustrates that this can be accomplished using $P^c_{nr}(t)$ without explicitly accounting for each molecule's spatial coordinates.

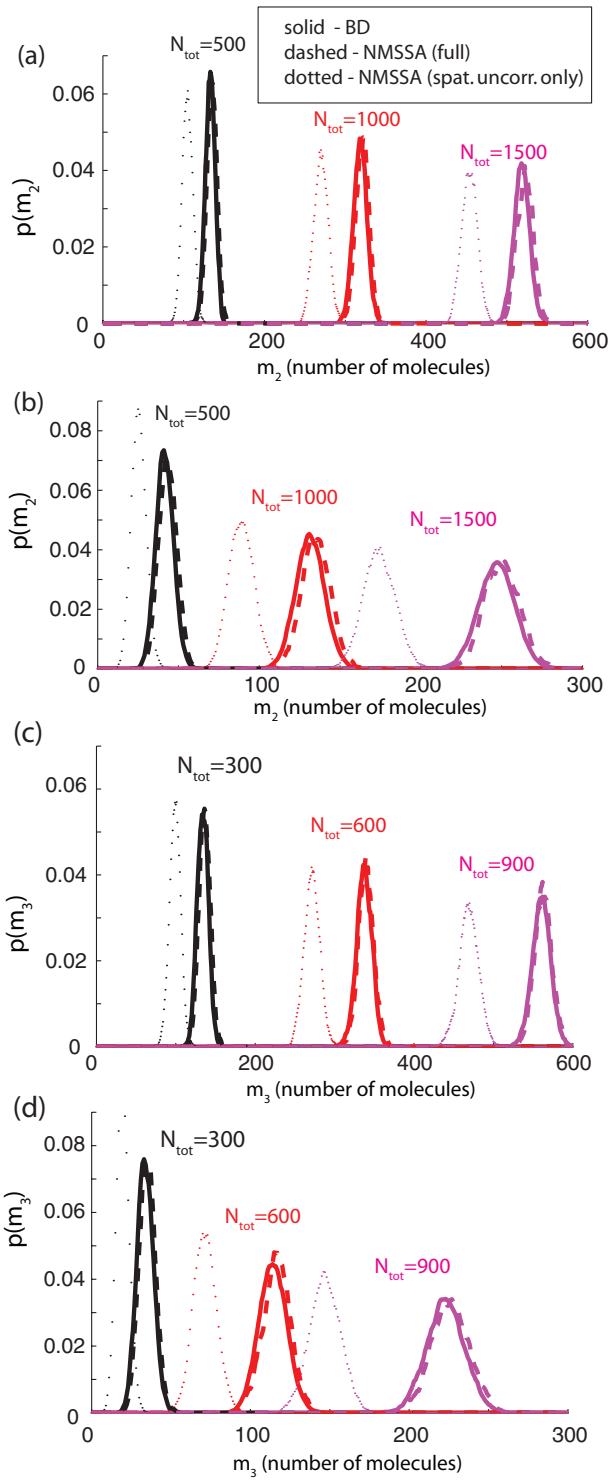

FIG. 5. Dissociation/reassociation system: Stationary distributions of the molecular-complex species (M_2 (homodimer), M_3 (heterodimer)). (a) Homodimer system with $\gamma_d = 100$. (b) Homodimer system with $\gamma_d = 1000$. (c) Heterodimer system with $\gamma_d = 100$. (d) Heterodimer system with $\gamma_d = 1000$.

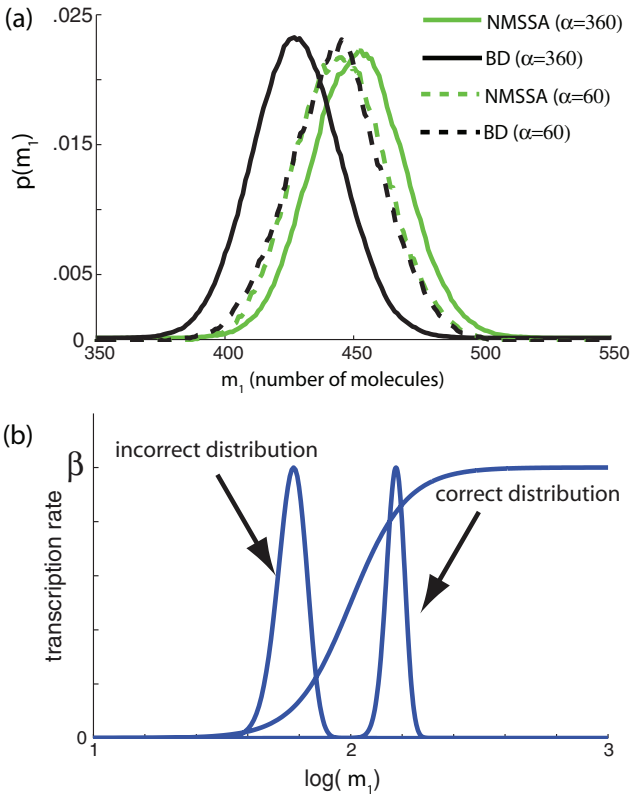

FIG. 6. (a) Annihilating homo-dimerising reacting system. Stationary distributions of M_1 computed using either the BD or NMSSA for $R/d_b = 100$ for $\alpha = 360$ and 60. (b) Implications of incorrectly calculating protein distributions. For this example, improperly calculated distribution underestimates downstream gene-expression.

C. Reacting system of annihilating homodimers

To test the limitation of NMSSA, we considered a final example where two molecules of M_1 can homo-dimerize and this dimerization leads to their annhibilation

$$M_1 + M_1 \rightarrow \emptyset, \tag{20a}$$

$$\emptyset \rightarrow M_1. \tag{20b}$$

For this system, monomer M_1 are the active form of the molecule and their dimerization (annihilation) can be considered as a deactivation or removal from the signalling system.

The M_1 synthesis rate, β_{m_1}, is set to drive the distribution means to near 450 molecules with $R/d_b = 100$. First, we consider the case of isotropic M_1 molecules ($\alpha = 360$). Indeed, the NMSSA distribution is shifted to the right of the BD distribution (Figure 6(a)). This discrepancy is likely to be an extreme manifestation of the effect of spatial fluctuations which cannot be captured by the NMSSA. In this case, the M_1 molecules can never cluster together on average as they annihilate each other. This produces a faster average mean diffusion reaction time. Thus, the BD calculations, which account for the spacing, show a lower mean in their distributions relative to the NMSSA results.

To test whether this limitation can be alleviated by increasing the mixing in the system through the presence of reaction surfaces on the molecules, we repeated the simulations for $\alpha = 60$. Here again, the NMSSA and BD distributions agree more closely (Figure 6(a)) reflecting that as α decreases, the system becomes more well-stirred due to the unproductive collisions involving the M_1 molecules. However, the system at $\alpha = 60$ is non-memoryless (it uses the same waiting distribution as the absorber system ($\alpha = 60$ in Figure 4(d)).

V. SUMMARY AND DISCUSSION

In this work, we developed a hybrid analytical/Brownian dynamics framework for calculating diffusion-reaction waiting time distributions, $\widetilde{P}^u_{nr}(t)$ and $\widetilde{P}^c_{nr}(t)$, on biological membranes for reacting molecules. We used these results to formulate an extension of the stochastic simulation algorithm (SSA) to accommodate diffusion-induced non-memoryless effects. We demonstrated that the NMSSA constitutes an accurate framework for studying systems involving diffusion on membranes for a wide array of parameter regimes, without the need to account for the spatial coordinates of the reacting molecules. Through direct comparison with BD simulations, we also documented scenarios where large spatial fluctuation effects mandate explicit consideration of all the molecules and their positions. These effects were particularly apparent in situations where low numbers of isotropic molecules of the same type can bind to each other. For orientation-dependent reactions, smaller reactive surface areas on the molecules caused the system to converge towards memoryless behavior, agreeing with the dogma that situations in which numerous unproductive collisions occur between reacting molecules allows the system to re-mix constantly.

These insights, while important to gain a fundamental understanding of the role of diffusion and spatial fluctuations in the simple systems considered, also provide a general computational methodology for simulating a broad class of biological networks where spatial effects might be important. This is essential for the proper modeling and quantification of signaling dynamics that rely heavily on a sensing step through membrane-bound receptors. For instance, if the M_1 molecules in the examples presented represent membrane receptors whose function is to convey an environmental signal to the cell's nucleus through the activation of a transcription factor, then accounting for their accurate statistics is crucial, in particular when either the activation of the transcription factor or the subsequent gene activation is a nonlinear function of M_1 (e.g., a routinely used Hill function, Figure 6(b)). In this case, improperly calculating the distribution of M_1 will lead to large errors in our assessment of gene activation and all subsequent steps.

In terms of efficieny, the NMSSA is at least 500 times faster than BD in all cases but still orders of magnitude slower than the SSA, particularly at high molecular numbers. However, given that the SSA is not applicable in most of the scenarios we modeled, the loss of efficiency of NMSSA compared to the SSA is justified. Moving forward, it will be interesting to derive an NMSSA-associated master equation which, much like the SSA-associated chemical master equation (CME), would enable analytical insight and faster Monte Carlo algorithms such as tau-leaping and time-dependent moment equations.

Recently, propensity functions for 3D diffusion reactions were developed assuming steady-state diffusion reactions.[25] This regime results in exponentially distributed reaction probabilities which can directly be used in the original SSA. Together with this work, our new framework provides a realistic means to simulate many types of biochemical cellular networks while accounting for molecular diffusion. Methods of this type will be necessary to understand the intricate interplay of space, diffusion, and reactions in biological systems.

ACKNOWLEDGMENTS

This work was supported by National Science Foundation (Grant Nos. CCF-0943385 and NCI U54 CA143836) to H.E. We would like to thank Charles Biddle-Snead for many useful discussions and critical reading of the manuscript.

APPENDIX A: BROWNIAN DYNAMICS SIMULATIONS

The Brownian dynamics algorithm used to analyze the systems in this paper is comprised of several components: diffusive transport, collision-reactions between molecules and creation/decay of molecules. We discuss the approaches for each of the components, and finally the algorithm itself.

1. Diffusive transport on sphere

Given the current position of each molecule at time t, the new position at time $t + \Delta t$ is updated through a simple random walk process. The coordinates of a given molecule are represented as $\vec{r}(t) = [x \;\; y \;\; z]^T$, in x, y, z cartesian coordinates where the origin is located at the center of the sphere. In traditional spherical coordinates, the variables $x = R\,\sin(\phi)\,\cos(\theta)$, $y = R\,\sin(\phi)\,\sin(\theta)$, $z = R\,\sin(\phi)\cos(\theta)$.

Before we perform the random walk process, we first transform the molecule coordinates to a local coordinate system $\vec{r}'(t) = [x'(t) = 0 \;\; y'(t) = 0 \;\; z'(t) = R]^T$. The transformation matrix between the two coordinate systems is

$$U = \begin{pmatrix} \cos(\phi)\cos(\theta) & \sin(\phi)\cos(\theta) & -\sin(\theta) \\ -\sin(\phi) & \cos(\phi) & 0 \\ \cos(\phi)\sin(\theta) & \sin(\phi)\sin(\theta) & \cos(\theta) \end{pmatrix}, \quad \text{(A1)}$$

where the matrix is unitary such that $\vec{r}'(t) = U\vec{r}(t)$ and $\vec{r}(t) = U^T\vec{r}'(t)$.

We next apply a random walk operation to calculate $\vec{r}'(t + \Delta t)$. To obtain $\vec{r}'(t + \Delta t)$, we begin by determining θ' and ϕ' at time $t + \Delta t$ by sampling the following pdf:

$$p(\theta', \phi') = \frac{\theta' R^2}{4\pi D_p \Delta t} \exp\left(-\frac{(\theta' R)^2}{4 D_p \Delta t}\right), \quad \text{(A2)}$$

which represents the distribution of molecule locations allowed to diffuse with diffusion coefficient D_p during a time Δt assuming a flat membrane. The pdf is explicitly a function of θ', and a uniform distribution in ϕ'. The flat membrane assumption is accurate for the sphere in this case, because Δt is always chosen such that $\theta' R \ll r_p \ll R$, and is small enough such that the spread of $p(\theta', \phi')$ is still within a locally flat region (no curvature effects) of the sphere. With θ' and ϕ' sampled we calculate the new coordinates: $x' = R\cos(\phi')\sin(\theta')$, $y' = R\sin(\phi')\sin(\theta')$, $z' = R\cos(\theta')$. We then transform back to the global coordinate system with $\vec{r}(t + \Delta t) = U^T\vec{r}'(t + \Delta t)$.

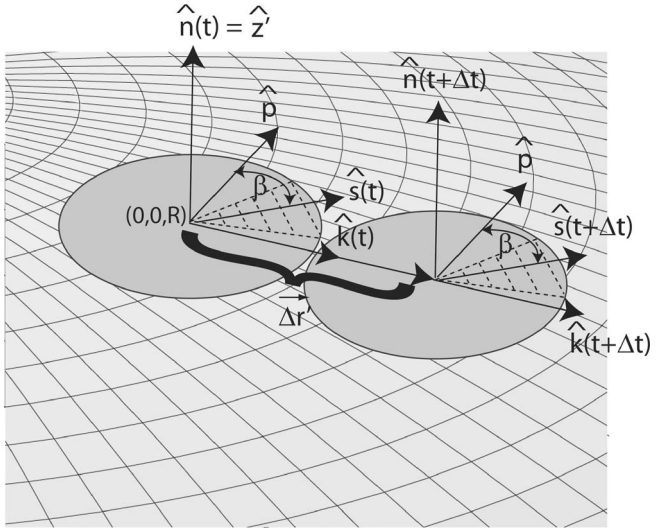

FIG. 7. Diagram of the translational random walk for the orientation-dependent reacting molecules.

For the orientation dependent reactions, we must also apply a rotational random walk to the molecule. The rotational random walk is applied after the translational random walk above. Figure 7 illustrates the molecule location in the local coordinate system at time t and $t + \Delta t$, i.e., before and after the translational random walk, but before the rotational random walk is applied. By definition the normal vector at time t is $\hat{n}(t) = [0 \;\; 0 \;\; 1]^T$, while the normal vector at time $t + \Delta t$ is $\hat{n}(t + \Delta t) = [\cos(\phi')\sin(\theta') \;\; \sin(\phi')\sin(\theta')\hat{y}' \;\; \cos(\theta')]^T$. The translational displacement vector is $\vec{\Delta r}' = \vec{r}'(t) - \vec{r}'(t + \Delta t) = [R\cos(\phi')\sin(\theta') R\sin(\phi')\sin(\theta') R(\cos(\theta') - 1)]^T$. We define $\hat{p} = \frac{\hat{n}(t)\times\hat{n}(t+\Delta t)}{|\hat{n}(t)\times\hat{n}(t+\Delta t)|} = [-\sin(\phi') \;\; \cos(\phi') \;\; 0]^T$, i.e., the normalized vector of the cross product between the normal vectors $\hat{n}(t)$ and $\hat{n}(t + \Delta t)$. This can also be interpreted as the unit vector normal to the great circle that intersects the tips of $\vec{r}'(t)$ and $\vec{r}'(t + \Delta t)$. The unit vectors tangent to the surface in the direction of translation at times t and $t + \Delta t$ are $\hat{k}(t) = \hat{p} \times \hat{n}(t) = [\cos(\phi')\hat{x}' \;\; \sin(\phi') \;\; 0]^T$ and $\hat{k}(t + \Delta t) = \hat{p} \times \hat{n}(t + \Delta t) = [\cos(\phi')\cos(\theta')\sin(\phi')\cos(\theta') \;\; -\sin(\theta')]^T$, respectively.

We define $\hat{s}(t)$ and $\hat{s}(t + \Delta t)$ as the direction from the center of the molecule to the center of the reacting surface (dashed line region) for times t and $t + \Delta t$, respectively (Figure 7). By definition $\hat{s}(t) = \cos(\beta)\hat{p} + \sin(\beta)\hat{k}(t)$. In order to apply rotational diffusion we must first calculate $\hat{s}(t + \Delta t)$. Because there is no rotation during translation we enforce that $\hat{s}(t + \Delta t) = \cos(\beta)\hat{p} + \sin(\beta)\hat{k}(t + \Delta t)$. We next apply rotational diffusion to $\hat{s}(t + \Delta t)$. The rotational diffusion coefficient is D_{rot}. The angular displacement $\Delta\beta$ due to the rotational random walk is drawn from the distribution $p(\Delta\beta) = \frac{1}{\sqrt{4\pi D_{rot}\Delta t}} \exp\left(\frac{(\Delta\beta)^2}{4D_{rot}\Delta t}\right)$ with the final vector for the reacting surface direction being $\hat{s}_f(t + \Delta t) = \cos(\beta + \Delta\beta)\hat{p} + \sin(\beta + \Delta\beta)\hat{k}(t + \Delta t)$. Finally, $U^T\hat{s}_f(t + \Delta t)$ transforms the vector back to the global coordinate system.

2. Collisions/reactions

After the molecules have undergone diffusive transport to time $t + \Delta t$, the relative distance between molecule positions of all the molecules with respect to each other are calculated. This is done to determine if any molecule set i, j are overlapping, i.e., $|\vec{r}_i - \vec{r}_j| <= r_{pi} + r_{pj}$, where r_{pi} and r_{pj} are the molecule radii of molecule i and j, respectively. If there is an overlap, there are two possible consequences. The first is that the two can react and their reaction product is formed at the location of their center of mass (for orientation-dependent reactions, their reacting surfaces must also be touching). The second is that they do not react in which case we apply their trajectories from time t to $t + \Delta t$ as a simple ballistic collision between two billiard balls, where the molecules collide and reflect off of each other.

3. SSA reactions

Stochastic creation of membrane molecules, e.g., M_1 and M_2, as well as decay/removal of M_2 molecules are calculated using a memoryless SSA algorithm. To accommodate for interfacing with NMSSA reactions, we use a slightly different procedure to calculate the memoryless reactions than in the typical SSA implementation. Memoryless reactions $P_{nr}(\tau - t)$ are first calculated at $\tau = t + \Delta t$. A random variable m is drawn from a uniform distribution between zero and one. If $m > P_{nr}(\Delta t)$ then no memoryless reaction occurred between t and $t + \Delta t$. However, if $m \leq P_{nr}(\Delta t)$, we must sample the time at which the reaction occurred from the conditional probability distribution $P_{nr}(\tau - t)/P_{nr}(\Delta t)$, as well as determine which reaction occurred. This is followed by updating the state x and time $t_s = t + \lambda \Delta t$, with $\lambda \leq 1.0$. The process would be repeated until $t_s = t + \Delta t$. For SSA reactions that involve membrane molecule(s), the particular membrane molecule(s) involved must be randomly sampled. If the SSA reaction results in the dissociation of a membrane molecule complex into two membrane molecules that can re-associate, the initial dissociation condition d_r, $\Delta\phi_r$ (Sec. II C) is applied. If the SSA reaction results in the creation of a new membrane molecule, that molecule must be randomly placed onto the membrane without overlapping any other molecules. If the SSA reaction results in the decay membrane molecule, the particular molecule that decays must be sampled and then removed.

4. Hybrid BD/SSA algorithm for diffusion reactions on a sphere

For each timestep, we first update the diffusion-reactions, followed by any memoryless reactions (creations, removals) that might have happened over the duration Δt. In theory, we are introducing a small error in that any state change that occurs due to a reaction occurring for a given stage update is carried to the next stage update, rather than updating each stage independently and adding up the contributions from each state at the end of the timestep. For this paper, Δt is sufficiently small such that tens to hundreds of timesteps typically occur between each reaction (diffusion-reaction, memoryless SSA reactions).

Algorithm:

Initialize molecules and their respective states and locations (no overlap) on sphere. Set time $t = 0$. Go to 1.

1. **Diffusive transport:** Update molecules positions (and rotations if orientation-dependent) over a timestep. Go to 2.
2. **Collision/Reactions:** Update any reaction products for any diffusion-reactions ($X = X + \nu_j$, given the reaction j). Update molecule populations as necessary. Readjust molecule positions for colliding, non-reacting molecules. Go to 3.
3. **Memoryless reactions:** Update any memoryless reactions that may have occurred during from t to Δt. The state of the system is readjusted after each reaction ($X = X + \nu_j$, given the reaction j). Update molecule populations as necessary. Go to 4.
4. $t = t + \Delta t$. If continue goto 1, otherwise, exit.

APPENDIX B: BROWNIAN DYNAMIC/ANALYTICAL APPROACH TO DETERMINE THE MICROSCOPIC RATE CONSTANT *k*

The basic assumption imposed in this work is that for orientation dependent reacting molecules, the microscopic rate constant parameter parameter k incorporates the effects of the reactions surfaces (α_1 and α_2), the molecular dimensions, and the relative relationship between the translational and rotational diffusion coefficients. In this section, we show this to be empirically true by using a iterative procedure to determine k. Note that if we run this problem in the reference frame of molecule M_1, the problem is radially symmetric in the xy plane (Figure 8(a)). That is, all we need to do is rotate the molecule M_2, azimuthally about M_1 (at the origin (0,0), orientation of M_1 rotates accordingly) at the fixed distance r_0 and run the problem. This will allow us to connect the results of BD to the analytical solution described in Sec. II.

We start with the reacting molecules M_1 and M_2 a fixed distance r_0 apart, where for this paper $r_0 = 5d_b$. The orientation of each molecule is randomly chosen. Using the Brownian dynamics algorithm discussed in Appendix A, we apply both translation and rotational random walks to the molecules given their diffusion coefficient values. We record the relative distance between the two molecules over time until they react (or until some maximum time is reached). We repeat the process for a large number of trials and compute $C_2(d, t = t_s) = \int_{d_b}^{d} p_2(d', t = t_s) dV'$, the fraction of trial instances where the M_2 molecule is between $d_b \leq d' \leq d$ at time t_s (Figure 8(b)) for a range of d values. $C_2(d, t = t_s)$ can then be approximated using a third order spline fitting procedure (Figure 8(b), green curve), and then differentiated to yield $\tilde{p}_2(d, t = t_s)$, an approximation of $p_2(d, t = t_s)$ (Figure 8(c)). For a given value of k, we plug $\tilde{p}_2(d, t = t_s)$ into Eq. (3) to obtain the eigenfunction amplitudes, A_n. This allows us to compute $\widetilde{P}_{nr}^{c}(t)$ analytically for $t \geq t_s$. We then compare $\widetilde{P}_{nr}(t)$ for $t > t_s$ between analytical case for the given k and $\widetilde{P}_{nr}(t)$ calculated using BD. The process is repeated, iteratively adjusting k, until the two approaches agree (computations done in MATLAB). For the simulation parameters from Sec. IV,

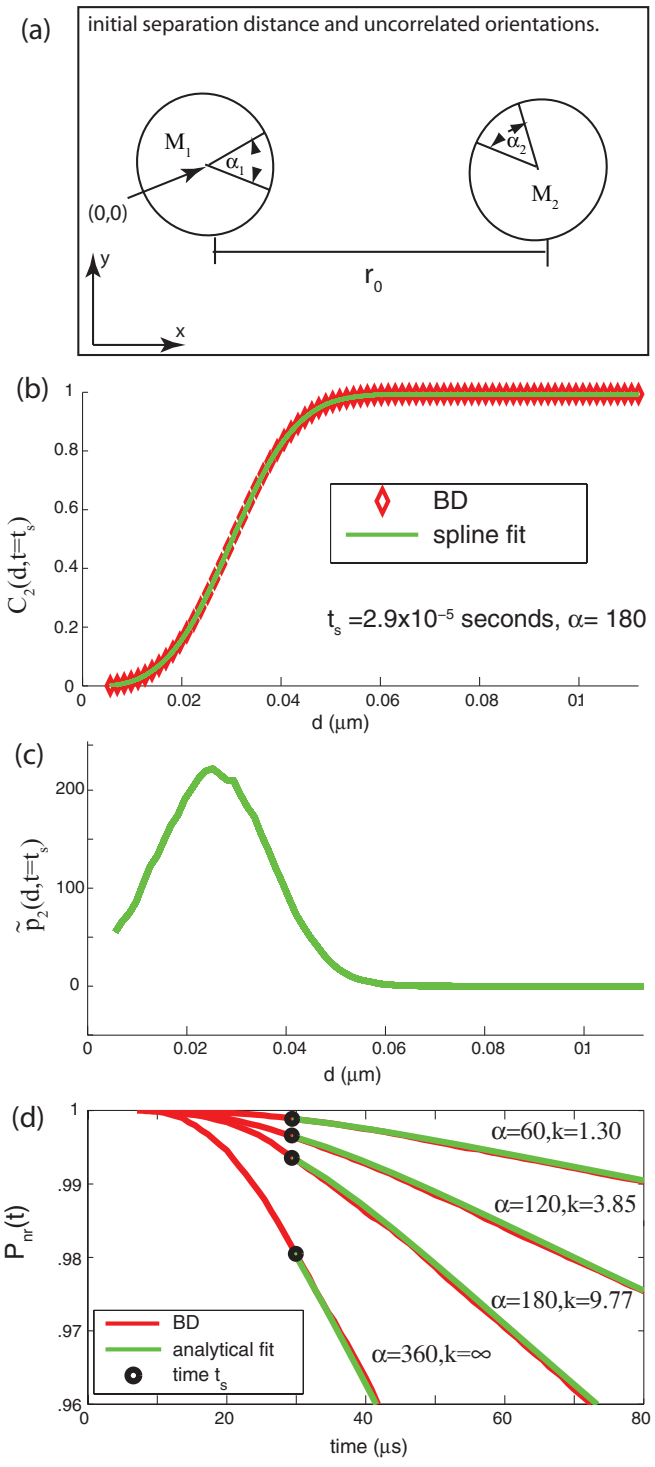

FIG. 8. Analytical/BD approaches for fitting the microscopic rate constant k: (a) Initial conditions. (b) $C_2(d, t = t_s)$ at time $t = t_s$ where $t_s = 2.9 \times 10^{-5}$ and $\alpha = 180$. (c) Spline fitted function $\tilde{p}_2(d, t = t_s)$. (d) Analytical solutions with fitted k vs. results of BD simulations.

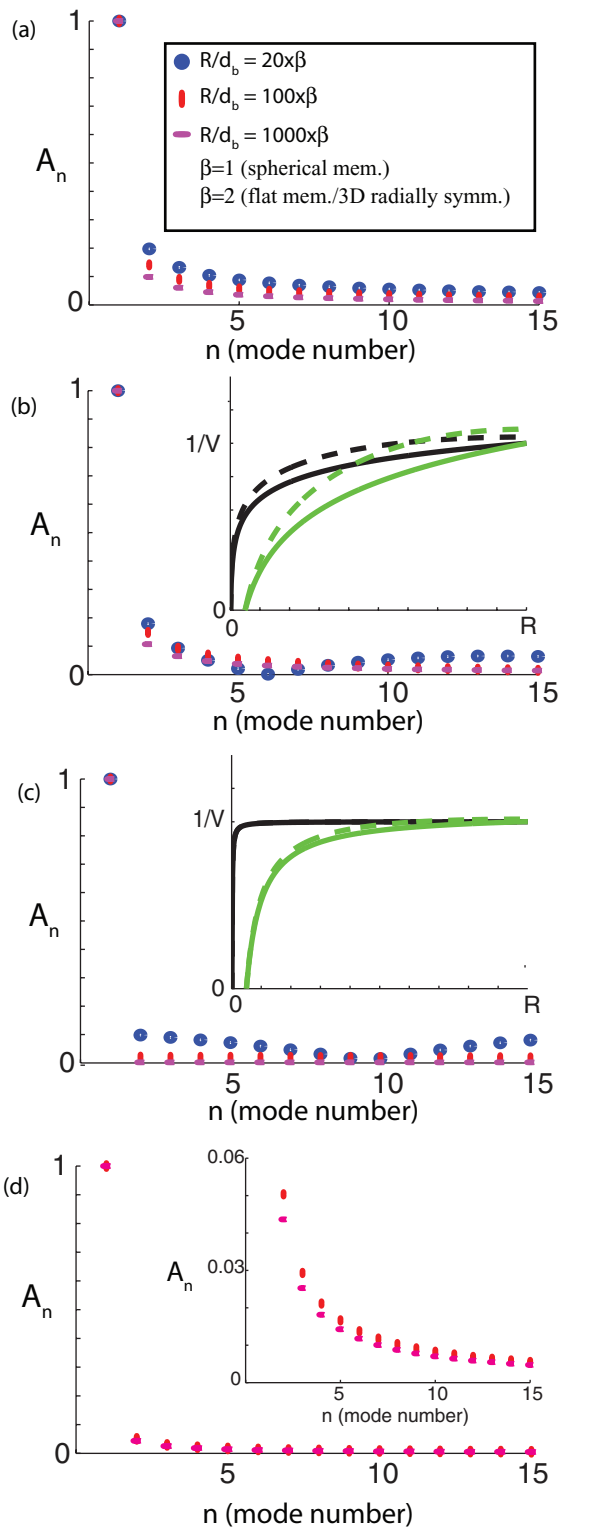

FIG. 9. Eigenfunction contributions, A_n,for the well mixed case. (a) Distributions of A_n vs. n for $R/d_b = 20$, 100, 1000 for the 2D spherical shell ($k = \infty$). (b) A_n vs n for $R/d_b = 40$, 200, 2000 in 2D cylindrically symmetric case ($k = \infty$). (c) A_n vs n for $R/d_b = 40$, 200, 2000 in 3D radially symmetric case ($k = \infty$). Insets in (b) and (c) are plots of the fundamental mode (dashed) vs. classic steady state solution (solid) for $R/d_b = 20$ (green) and $R/d_b = 1000$ (black), all for $k = \infty$. (d) Distributions of A_n vs. n for $R/d_b = 100$, 1000 for the 2D spherical shell ($k = 1.30$ corresponding to $\alpha_1 = \alpha_2 = 60$). Inset is a zoom in of A_n for $n = 2$ to 15.

Figure 8(d) shows fits for $\alpha_1 = \alpha_2 = \alpha = 360^\circ$, 180°, 120°, and 60° and where the resulting k values are $k = \infty$, 9.77, 3.85, and 1.30, respectively. The two approaches agree well in all cases.

For this paper, we are focused on 2D membrane molecules, but this approach for fitting k is easily extended to 3D as well. In addition, the approach should be applicable

to fitting k for reactions between higher resolution protein structures using full molecular dynamics simulations, which include diffusion, electrostatics, etc. The values of k for a given reacting molecule pair is fundamental and can be applied to any algorithm[12–14] that uses analytical approaches that require the Collin and Kimball[7] partially reflecting boundary condition.

APPENDIX C: ANALYSIS OF EIGENFUNCTION COEFFICIENTS, A_n, FOR THE SPATIALLY UNCORRELATED WAITING TIME DISTRIBUTION

Here, we further analyze the multiple timescales of $\widetilde{P}^u_{nr}(t)$ by comparing the eigenfunction coefficients A_n for the spherical membrane and flat membrane cases of the same surface area. We start with the $k = \infty$ case, which represents a system in which all collisions between the two reacting molecules result in a reaction. A_n for the first 15 modes of the spherical membrane case are shown in Figure 9(a) using $R/d_b = 20$, 100, and 1000. In all cases, higher order modes can be seen to significantly contribute to the solution, illustrating that multiple exponential timescales contribute to the behavior of this system where molecules are confined to diffuse on a 2D surface.

For the flat membrane case, A_n are shown for the first 15 modes in Figure 9(b), respectively, for $R/d_b = 40$, 200, and 2000. The flat membrane case and the spherical membrane results are similar in that the higher order modes significantly contribute to the solution for any R/d_b.

Our framework also allows us to address different spatial dimensions, specifically 2D vs. 3D. It turns out that the 2D flat membrane (radially symmetric) eigenfunction solutions are easily translated to the 3D radially symmetric case, representing diffusion-reactions within the 3D cytosol. For the 3D radially symmetric case, the volume is $V = (4/3)\pi[R^3 - d_b^3])$ and the eigenfunctions are spherical bessel functions of the first and second kind. We use the same diffusion coefficient and molecular dimensions (3D molecules in this case) with $k = \infty$. For the 3D case (Figure 9(c)), the contribution of higher modes is significant for $R/d_b = 40$, but the first mode increasingly dominates for $R/d_b = 200$ and 2000. In these cases, $\widetilde{P}^u_{nr}(t)$ becomes approximately memoryless. This point is also underscored by results in the insets of Figures 9(b) and 9(c) which plot the fundamental mode (dashed) and the classic stationary solution (solid) for $R/d_b = 20$ (green) and $R/d_b = 1000$ (black) for 2D flat membrane and 3D radially symmetric case, respectively. The stationary solution are $\log(d/d_b)/\log(b/d_b)$ (2D) and $\frac{1/a-1/d}{1/a-1/R}$ (3D). Therefore, diffusion in 3D tends to alleviate the non-memoryless nature of the solution for spatially uncorrelated reactions.

Finally, we analyzed the eigenfunction coefficients A_n for the case $k = 1.30$, which corresponds to partially reflecting molecules of $\alpha_1 = \alpha_2 = 60$ (see Appendix B). The spherical membrane case for $R/d_b = 100$ and 1000 are plotted (Figure 9(d)) where the relative contributions of the higher order eigenfunction are smaller than that of the $k = \infty$ case, but are still present. In fact, there is little difference between the $R/d_b = 100$ and 1000 cases. For $k = 1.30$, the results for the flat membrane case at $R/d_b = 200$ and 2000 (results not plotted) are very similar to the spherical membrane case. For the 3D radial case ($k = 1.30$) both for $R/d_b = 200$ and 2000 (results not plotted) the fundamental eigenfunction dominates (memoryless) as it did for the case where $R/d_b = 2000$ and $k = \infty$ above. In summary, for large enough R/d_b, diffusion-reactions in 3D are approximately memoryless, the widely used memoryless assumption in stochastic chemical kinetics (e.g., Ref. 15), while for 2D membranes, accounting for diffusion dynamics violates the widely used memoryless assumption.

[1] S. Halford and J. Marko, Nucleic Acids Res. **32**, 3040 (2004).
[2] G. Tkacik and W. Bialek, Phys. Rev. E **79**, 051901 (2009).
[3] H. Berg and W. Purcell, Biophys. J. **20**, 193 (1977).
[4] T. Gregor, D. Tank, E. Wieschaus, and W. Bialek, Cell **130**, 153 (2007).
[5] D. Pincus, M. Chevalier, T. Aragón, E. van Anken, S. Vidal, H. El-Samad, and P. Walter, PLoS Biol. **8**, e1000415 (2010).
[6] M. Smoluchowski, Z. Phys. Chem. **92**, 129 (1917).
[7] F. Collins and G. Kimball, J. Colloid Sci. **4**, 425 (1949).
[8] F. Collins and G. Kimball, Ind. Eng. Chem. **41**, 2551 (1949).
[9] A. Szabo, J. Phys. Chem. **93**, 6929 (1989).
[10] N. Batada, L. Shepp, D. Siegmund, and M. Levitt, PLOS Comput. Biol. **2**, e44 (2006).
[11] H. Kim and K. Shin, Phys. Rev. Lett. **82**, 1578 (1999).
[12] S. Andrews and D. Bray, Phys. Biol. **1**, 137 (2004).
[13] S. Andrews, N. Addy, R. Brent, and A. Arkin, PLOS Comput. Biol. **6**, 1000705 (2010).
[14] J. van Zon and P. ten Wolde, Phys. Rev. Lett. **94**, 128103 (2005).
[15] D. Gillespie, J. Comp. Phys. **22**, 403 (1976).
[16] R. Erban and J. Chapman, Phys. Biol. **06**, 046001 (2009).
[17] D. Fange, O. Berg, P. Sjoberg, and J. Elf, Proc. Natl. Acad. Sci. U.S.A. **107**, 19820 (2010).
[18] S. Hellander, A. Hellander, and L. Petzold, Phys. Rev. E **85**, 042901 (2012).
[19] P. Saffman and M. Delbruck, Proc. Natl. Acad. Sci. U.S.A. **72**, 3111 (1975).
[20] J. Jackson, *Classical Electrodynamics* (Wiley, New York, 1999).
[21] B. Barrowes, *Computation of Special Functions* (MathWorks, Natick, MA, 2004).
[22] S. Zhang and J. Jin, *Computation of Special Functions* (Wiley, 1996).
[23] B. Barrowes, *The Multiple Precision Toolbox for Matlab* (MathWorks, Natick, MA, 2004).
[24] M. Puthenveedu, B. Lauffer, P. Temkin, R. Vistein, P. Carlton, K. Thorn, J. Taunton, O. Weiner, R. Parton, and M. von Zastrow, Cell **143**, 761 (2010).
[25] D. Gillespie, J. Chem. Phys. **131**, 164109 (2009).